Highly confined excitons in MgS/ZnSe quantum wells grown by molecular beam epitaxy

C. Bradford, C. B. O'Donnell,* B. Urbaszek, C. Morhain,† A. Balocchi, K. A. Prior, and B. C. Cavenett
Department of Physics, Heriot-Watt University, Edinburgh, EH14 4AS, United Kingdom
(Received 30 March 2001; published 15 October 2001)

MgS has been grown by molecular beam epitaxy in the zincblende crystal structure on GaAs (100) substrates using a technique where the sources are Mg and ZnS. Layers up to 134 nm thick have been grown without any degradation in the crystal structure. The lattice constant was found to be 0.5619 ± 0.0001 nm and Poisson's ratio was estimated to be 0.425. The success of this growth technique has allowed the fabrication of MgS/ZnSe/MgS quantum wells that show sharp photoluminescence and transmission spectra indicating less than 1 ML fluctuations of the well widths. The small inhomogeneous broadening of the samples has allowed magneto-optical studies of the exciton absorption where the observation of higher excited exciton states have been observed and the exciton binding energies, E^X, have been measured directly, notably $E^X(1s-2s) > h\nu_{\mathrm{LO}}$ in a 5 nm well. The full width at half maximum of the heavy-hole absorption transitions for this sample has been measured as a function of temperature and no broadening of the excitonic transitions has been observed up to 150 K showing that the exciton-LO phonon scattering has been suppressed.

DOI: 10.1103/PhysRevB.64.195309 PACS number(s): 81.15.Hi, 71.35.Cc, 78.55.Et, 61.10.Eq

I. INTRODUCTION

The compound MgS has a number of interesting properties that have made it the focus of attention for many years. Although its stable crystal structure is the rocksalt (NaCl) phase, the Philips' ionicity of MgS is 0.786, close to the boundary between the regions of stability for the NaCl and zincblende (ZB) phases. In fact, it was shown by Navrotsky and Philips[1] that the free energy for the transformation between the NaCl and ZB phases is close to zero. *Ab initio* calculations by Lichanot *et al.*,[2] however, suggested that at 0 K and zero pressure, the ZB structure is the more stable, with the transition to the NaCl structure occurring at $P=1$ GPa. However, Ekbundit *et al.*[3] calculated that the NaCl structure was the most stable at zero pressure, although under tension both the wurtzite and ZB crystal phases were stabilised. ZB MgS is a particularly interesting compound since theoretical calculations[4] give a lattice constant for this compound close to that of both GaAs and ZnSe and this has been supported by values of the lattice constant extrapolated from ZnMgS alloys containing mole fractions of Mg up to 0.14.[5] Above this value, a change in the crystal structure from ZB to NaCl was observed.

The low strain of ZB MgS with GaAs makes the growth of epitaxial MgS/ZnSe/MgS quantum well structures on GaAs substrates a possibility with the attraction of a barrier with an energy of $\sim$5 eV. However, the first attempt to grow ZB MgS by molecular beam epitaxy (MBE) obtained layers only 0.96 nm thick before there was a sharp transition from two-dimensional (2D) to 3D growth observed by reflection high-energy electron diffraction (RHEED). This was attributed to a change in the crystalline structure of the epitaxial layer.[6] MgS has also been grown using metal-organic chemical-vapor deposition (MOCVD) on GaAs (100) substrates and in layers that were approximately 2 μm thick both ZB and NaCl phases were detected by x-ray diffraction.[7] However, in much thinner MOCVD-grown layers (up to 10 nm thick) the ZB structure was maintained.[8] The crystalline quality of these layers was sufficiently good for use as barriers with ZnSe quantum-well layers, which showed large carrier confinement and excitonic spectra observable[9,10] up to room temperature.

More recently we have grown MgS by MBE using a method that utilizes ZnS and Mg sources. This method has proved successful and has allowed us to report the growth of layers up to 67 nm thick with excellent crystalline quality.[11] In this paper, we describe the growth method together with improvements in the growth technique that have enabled us to grow ZB layers of MgS even thicker than those described previously. Second, we report details of the structural characterization of the layers by double-crystal x-ray rocking curves (DCXRC) and give details of the stability of the layers and the reactions that give rise to MgS. Finally, we discuss the growth of MgS/ZnSe quantum-well structures and the measurements of photoluminescence (PL) and magnetotransmission spectra in order to explore the suppression of exciton-LO phonon scattering when the exciton binding energy $E^X(1s-2s) > h\nu_{\mathrm{LO}}$.

II. GROWTH OF MgS

All the MgS and ZnSe layers were grown in a Vacuum Generators V80H MBE system using 6 N Mg, Zn, and Se elemental sources and a ZnS compound source. No modifications were made to the MBE system, however, a liquid-nitrogen cooled shutter was fitted in front of the ZnS cell. This was done to reduce substantially the amount of ZnS leaking around the shutter when the cell is hot and the subsequent contamination of the growth chamber by sulphur containing species. With the cooled shutter fitted, we are able to reproducibly clean GaAs substrates and cool them to below 300 °C under a Zn flux,[12,13] while maintaining the 4$\times$ reconstruction along the [110] azimuth. This shows that there is no significant contamination by sulphur of the clean GaAs surface under these conditions.

MgS samples were grown on GaAs substrates that had been etched and heated to 580 °C to remove the oxide layer, then cooled to the growth temperature (typically 240–

 ©2001 The American Physical Society

270 °C), after which a 5–10 nm buffer layer of ZnSe was deposited. Typically, RHEED shows that the initial growth was 3D, subsequently transforming to the usual (2×1) RHEED pattern with long streaks observed from a ZnSe epitaxial layer. MgS was grown using Mg and ZnS sources with cell temperatures of 375 and 800 °C, respectively. The Mg flux was not routinely measured in order to minimize contamination of the ion gauge. Following the growth of the MgS layer, a capping layer of ZnSe typically 5–10 nm thick was deposited that was found to protect the MgS layer from oxidation.

During the course of this work, a variety of different sample structures were grown. First, thin samples, containing MgS layers less than 10 nm thick were used to determine the growth rate by x-ray interference techniques, as described in Sec. III A. Second, thick samples were used to determine the lattice constant and the residual zinc content and also to determine the maximum thickness that can be grown in the ZB structure, as described in Sec. III B. Finally, the quantum-well structures used for optical spectroscopy are described.

III. X-RAY CHARACTERIZATION OF MgS LAYERS

A. X-ray interference measurements of thin layers

In our initial work on MgS we identified a number of potential problems. First, the growth rate of MgS could not be determined, as it is well known that prolonged exposure to Mg rapidly causes the background current of an ion gauge to rise. It is presumed that this arises from electron-stimulated desorption from the ion gauge components that are covered with MgS. In addition, it was not thought that thick layers of the compound would be stable and hence layers thick enough to be measured with optical interference techniques could not be grown. Lastly, neither the composition nor the lattice constant of the material deposited were known and without thick layers to examine could not be determined.

In order to determine the growth rate and crystallinity of very thin MgS layers, we have used the method of x-Ray Interference (XRI).[14] In this method, the layer under examination forms the central spacer between two thicker layers of a different composition. Under these circumstances a Bragg interferometer is formed and the thin central layer modulates the intensity of the Pendellösung fringes. The pattern of modulation produced is a function of both the planar spacing of the central layer and its thickness, and repeats regularly with increasing thickness. This method has been described in detail elsewhere.[14,15,16]

In the present work we have used both 400 and 115 reflections because of the much larger strain between the two II-VI compounds than is found in the III-V system. This causes the pattern of modulation of the Pendellösung fringes that is observed in XRI to repeat more frequently with increasing layer thickness, and it is not possible to obtain an unambiguous choice of layer thickness. However, by using two reflections with different planar spacings, a unique value is obtained.[17]

The calculated thickness of the central layer does not depend on any previous knowledge of any structural parameters of the layer. We have thus been able to obtain the thickness of the layers and use these values to calculate the growth rate of MgS for layers <10 nm thick in structures of the type ZnSe(50 nm)/MgS(x nm)/ZnSe(50 nm), where 3 nm$\leqslant x \leqslant$10 nm. For a constant Mg cell temperature we observed that the growth rate was also constant within experimental error, and thus there is no variation in the Mg incorporation coefficient in thin samples. Previous work on ZnMgSSe alloys has also shown no variation in the Mg mole fraction throughout thicker layers, and we conclude that the growth rate obtained from these thin samples may safely be extrapolated to much longer growth times.

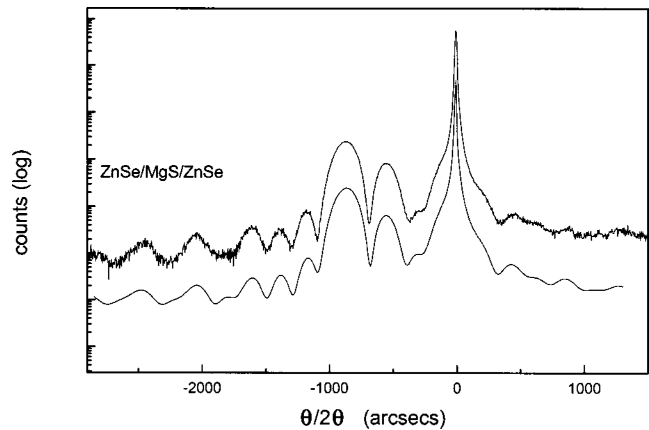

FIG. 1. X-ray interference pattern (top curve) and simulation (bottom curve) for the 400 reflection for a layer with the structure ZnSe (50 nm)/MgS (3 nm)/ZnSe (50 nm).

An example of a 400 reflection for a structure containing a 3 nm MgS layer is shown in Fig. 1, together with the calculated profile. The interplanar spacings obtained for the 400 and 115 reflections can be used with a_{MgS} (derived in Sec. III B) to obtain the Poisson's ratio, ν, and the amount of relaxation in the layers. However, these two values can not be obtained independently from these measurements. Previously, we used a value for the Poisson's ratio obtained from the calculated values of the elastic constants c_{11} and c_{12} by Chung *et al.*,[18] and estimated a 5–10% relaxation in the thin MgS layers.[11] Using ν as a variable parameter while the relaxation is simultaneously decreased improves the fit between the experimental and calculated rocking curves. The best fit was obtained with $\nu=0.425$ for a pseudomorphic MgS layer. Recently, c_{11} and c_{12} have been recalculated for MgS and the values obtained used to calculate the LO phonon frequency.[19] The calculated phonon frequency is in good agreement with the experimentally determined value and the calculated elastic constants also give $\nu=0.425$.

B. Determination of the lattice constant of MgS

Following the use of the XRI technique to determine the growth rate, a series of thicker MgS samples were grown on ZnSe buffer layers, as described in Sec. II. During growth, the MgS layers displayed (2×1) reconstructions with sharp streaks, indicative of flat surfaces and 2D growth, up to the point where the NaCl structure nucleates that was marked by a change to a spotty RHEED pattern.[6]

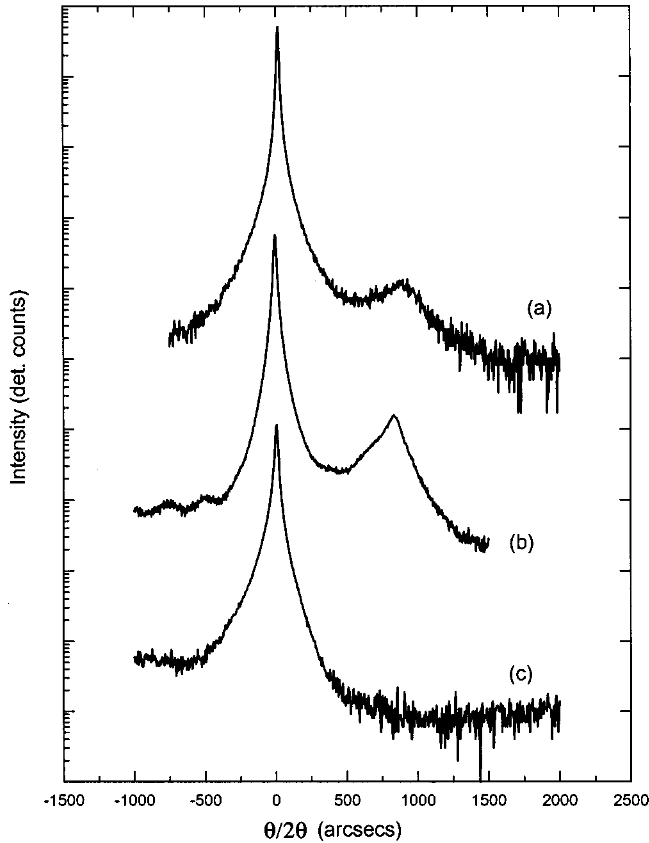

FIG. 2. 400 double-crystal rocking curves from samples with the following structures: (a) ZnSe (5 nm)/MgS (67 nm)/ZnSe (5 nm), (b) ZnSe (5 nm)/MgS (25 nm)/ZnSe (10 nm)/MgS (134 nm)/ZnSe (5 nm), (c) ZnSe (50 nm)/MgS (125 nm)/ZnSe (10 nm). The thickness of the MgS layer is a nominal value that the layer would have had if there were no transformation to the rocksalt phase.

The MgS layers that were deposited were sufficiently thick that their structural quality could be examined using DCXRC. Figure 2 shows the 400 data from two such samples grown at 240 °C. The first sample, shown in Fig. 2(a) has the structure ZnSe (5 nm)/MgS (67 nm)/ZnSe(5 nm) and has been reported previously.[11] During the growth of the MgS layers, as the only source of sulphur supplied is the ZnS flux, some residual Zn incorporation is to be expected. This particular sample was thick enough to allow analysis by secondary-ion-mass spectroscopy and Auger spectroscopy, which gave an estimate of the residual Zn content between 0.5 and 2%, allowing for the uncertainty in the sputtering coefficient of Mg. Also, in this sample, a comparison of the 400 and 115 reflections shows that it is 98% relaxed and has a lattice constant a of 0.5619 ± 0.0001 nm. Using Vegard's Law, and given that the residual zinc content of the sample lies in the range 0.5–2.0 %, we deduce a value for a_{MgS} in pure ZB MgS of 0.5622 ± 0.0002 nm. Table I gives the values for the lattice constant of MgS obtained from experimental work and previous theoretical calculations. We note that our value lies between the previous values obtained from much thinner layers grown by MOCVD of 0.559 (Ref. 8) and 0.566 nm (Ref. 7), respectively.

In order to see if the surface roughness influences the maximum thickness of MgS that can be grown on a ZnSe buffer layer h_{cp}, the ZnSe buffer layer was replaced by a ZnSe/MgS multilayer in the sample shown in Fig. 2(b). This sample has the structure ZnSe (5 nm)/MgS (25 nm)/ZnSe (10 nm)/MgS (134 nm)/ZnSe (5 nm). While both samples showed clear diffraction signals from the MgS layers, indicating that the layers retained the ZB crystal structure, the second structure appears to be of higher quality as it had only partially relaxed as indicated by the asymmetric shape of the DCXRC peak. The 134 nm thick MgS layer is the thickest grown in the ZB structure to date. Given the strains existing between the GaAs substrate and the ZnSe and MgS layers ($\epsilon_{\mathrm{ZnSe}} = -0.0025$, $\epsilon_{\mathrm{MgS}} = 0.0056$), and the fact that the onset of strain relief is usually observed in ZnSe after 150 nm, we would expect to see strain relief in MgS starting in layers over ≈70 nm thick, as is observed in the present case.

IV. STABILITY AND FORMATION OF MgS LAYERS

A. Stability of zinc blende MgS

In our preliminary study of the growth of ZB MgS,[11] we have noted a sharp transition between 2D and 3D growth and assigned this change to the onset of the nucleation of the rocksalt phase, in line with previous work.[6] We have found that the thickness at which this change occurs, h_{cp}, is a strong function of the sample growth temperature. At 240 °C, h_{cp} is 67 nm, while at 270 °C it is reduced to 12.5 nm.

TABLE I. Experimental and theoretical values of the lattice constant of zincblende MgS.

Method	Value (nm)	Reference
DXCRD, MgS	0.5622 ± 0.0002	This work
DXCRD, MgS	0.566	7
DCXRD, MgS	0.559	8
DCXRD, extrapolation in ZnMgSSe alloys	0.5643	5
Theory	0.546	4
Theory	0.573	2
Theory	0.561	20
Theory	0.562	21
Theory	0.549	22
Theory	0.5584	23

Layers of MgS thinner than h_{cp} are stable in the ZB phase almost indefinitely, even after prolonged exposure to the 15 kV RHEED beam. To determine the origin of the phase change, a layer of MgS 40 nm thick was grown at 240 °C. At this temperature the layer thickness was less than h_{cp}. Growth was then halted and the temperature raised in 10 K steps to 320 °C. At the higher temperatures, the layer thickness was substantially greater than h_{cp} but no change in crystal structure was observed by RHEED for times upto 1 h. From this, it may be concluded that the phase change is not nucleated in the bulk of the layer, but must occur at the surface during growth.

To determine whether the change observed in RHEED is the onset on the formation of the rocksalt phase, we have grown a layer thicker than h_{cp}. Figure 2(c) shows a 400 DCXRC trace from a MgS layer that was grown under similar conditions to the layer shown in Fig. 2(a), but on a thicker ZnSe buffer layer. After approximately 67 nm of ZB MgS was grown, RHEED clearly indicated a change from 2D to 3D growth. At this stage the growth was not terminated, but continued until the equivalent of 125 nm of ZB MgS was deposited, and the sample was then capped with 10 nm ZnSe. Although this sample is substantially thicker than the sample shown in Fig. 2(a), there is no trace of a ZB MgS peak.

The growth of pseudomorphic thin films in metastable phases has been of interest for many years, and calculations show that beyond a certain critical thickness a metastable layer should start to transform back to the stable bulk structure.[24,25] A number of systems have been analyzed, typically these have low strain between the two phases and are also diffusionless, such as bcc layers transforming to fcc. In semiconductors, the transformation of pseudomorphic ZnCdS grown on GaAs (001) from ZB to the wurtzite phase has been studied.[26] In this system it is found that the wurtzite phase nucleates preferentially on the very small twinned regions that expose a $(1\bar{1}1)$ plane at the crystal surface. Once nucleated, the wurtzite phase propagates in the growth direction, but does not transform the ZB layer either in the same plane or below it into more wurtzite phase crystal.

This transformation of zinc blende to wurtzite is similar to those transformations considered by Bruinsma and Zangwill.[25] It is diffusionless, and occurs by shearing across the common plane $(\{111\}_{ZB} \| \{0001\}_{NaCl})$. There is no strain between the ZB and wurtzite phases, and no change in the coordination number of any atom.

The transformation of ZB to rocksalt is quite different. Although there is a common plane relationship $(\{111\}_{ZB} \| \{111\}_{NaCl})$, the transformation mechanism is quite different. It can be thought of as a displacement of the cation and anion sublattices relative to one another along a $\langle 111 \rangle$ direction that changes the environments of both anion and cation from tetrahedral to octahedral coordination, and results in a large increase in density. The equivalent strain is approximately 13% in any direction.

With such a large change in volume, the resulting rocksalt MgS layer must induce cracks around the nucleation sites, which are possibly the features causing the sudden change from 2D to 3D diffraction observed in the RHEED patterns. From this, we may suggest two reasons why the ZB layer has disappeared in Fig. 2(c). First, propagation of the cracks into the ZB phase could cause the remaining MgS layer to adopt a range of tilts, becoming a mosaic structure and distributing the intensity over a wide angular range. However, as the ZB peak appears to have completely disappeared, and not merely reduced in intensity, a more likely explanation is that propagation of the cracks into the underlying ZB layer induces the complete transformation of the ZB phase to the more stable NaCl phase.

B. Replacement of Zn by Mg in the surface layer

The formation of MgS in the ZB crystal structure may occur by at least part of the impinging Zn flux becoming bonded at the surface, with the Zn atoms incorporating with the preferred tetrahedral bonding. Before the formation of the next layer, these Zn atoms are displaced by Mg atoms, which are then forced into a four-fold coordination, rather than the six-fold coordination found in the NaCl structure. The ZnS growth rate at 240–270 °C was measured in calibration samples to be 0.09 μm h^{-1}, while that of the MgS was measured to be 0.15 μm h^{-1}. This result can be explained by noting that the incorporation rate of sulphur on a growing ZnS surface is substantially lower than unity, while Mg is known to increase the incorporation of sulphur in ZnMgSSe alloys.[27] It was stated above that ZnS and Mg react exothermically at the semiconductor surface, forming MgS and liberating zinc, which does not incorporate substantially into the lattice. Here we examine that assumption by determining the equilibrium constants for the reaction of magnesium with ZnS and showing that it is compatible with a low residual zinc content. The growth rate of MgS corresponds to a Mg flux of 1×10^{14} atoms cm^{-2} s^{-1}. This is equivalent to an applied pressure of 4.5×10^{-7} mbar, which is less than the equilibrium vapor pressure of solid Mg at the growth temperature. Thus we calculate the equilibrium constants using the applied Mg pressure rather than the higher activity of solid Mg. We can now calculate the equilibrium constants for the reaction at the growth temperature. After substituting the activities of the MgS and ZnS alloy components and the Mg pressure, we obtain the pressure of Zn in equilibrium with that concentration of zinc in the alloy. We can then use this estimate of the Zn activity to determine whether these reactions are appropriate under MBE conditions.[29]

The reaction to consider is the displacement of Zn from solid ZnS by the applied Mg flux

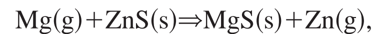

$$\mathrm{Mg(g)+ZnS(s)\Rightarrow MgS(s)+Zn(g)},$$

where the symbols (s) and (g) refer to the solid and gaseous phases, respectively.

The equilibrium constant for this reaction is K, where

$$K=\frac{p_{\mathrm{Zn}}a_{\mathrm{MgS}}}{P_{\mathrm{Mg}}a_{\mathrm{ZnS}}}. \qquad (1)$$

We assume to a first approximation that $Zn_xMg_{1-x}S$ is an ideal solid solution and the activities of MgS and ZnS are

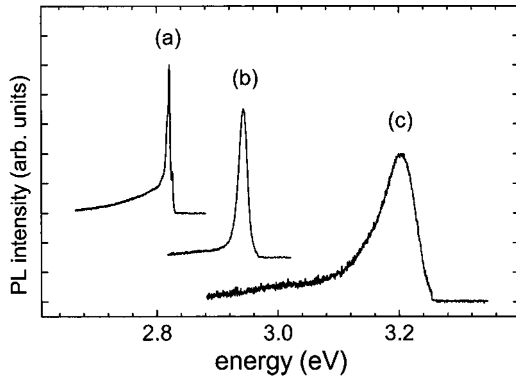

FIG. 3. PL spectra from single ZnSe quantum wells with well widths (a) 1.7 nm, (b) 3.3 nm, and (c) 10 nm.

given by their mole fractions, thus $a_{\mathrm{MgS}}=0.995$ and $a_{\mathrm{ZnS}}=0.005$ in the worst case, leading to the lowest incorporation of Zn.

The equilibrium constant is obtained from the Gibbs-free-energy changes for the reactions at the growth temperature, calculated from the entropy and enthalpy changes. For most chemical species, tabulated values of enthalpies and entropies at 298 K are available,[28] but accurate values at other temperatures require knowledge of the specific heat at constant pressure that is generally not available. A good estimate is made by substituting the values obtained at 298 K,[29,30]

$$-RT\ln K=\Delta G=\Delta H-T\Delta S\approx\Delta H_{298}-T\Delta S_{298}. \quad (2)$$

For ZB MgS there are no available thermodynamic data and we have used the values suggested by Sorokin *et al.*,[30] where the enthalpy has been calculated by reducing the value for the NaCl phase by one third to allow for the reduction in the coordination number.

We obtain $K=49\,000$ at 240 °C and at equilibrium we require a Zn overpressure of 10^{-4} mbar, which is somewhat in excess of the equilibrium pressure over pure Zn at this temperature. Although this calculated equilibrium constant is a very crude estimate, it is sufficiently large to give us confidence in the answers. The residual concentration of Zn in the solid is not an equilibrium concentration, but is rather determined by the kinetics of the reaction.

V. MgS/ZnSe/MgS QUANTUM WELLS

Due to the large difference, in excess of 2 eV, in bandgap between MgS and ZnSe and the possibility of growing multilayers of high structural and optical quality, this system is ideally suited for investigating strongly confined carriers by optical spectroscopy. Therefore, single quantum-well samples with structures ZnSe (buffer, 25–100 nm)/MgS(10 nm)/ZnSe(L_W nm)/MgS(10 nm)/ZnSe (cap, 3–10 nm) were fabricated with the growth temperature maintained at 240 °C throughout the growth. Values of L_W, the quantum-well widths, were chosen to be 1.7, 3.3, and 10.0 nm. PL spectra from these samples are shown in Fig. 3 where the spectral widths of the emission peaks are consistent with fluctuations of less than one monolayer at the interfaces. We have found excitonic emission at 3.2 eV for the narrowest well, corresponding to a confinement energy of 430 meV for ZnSe quantum wells. Exposure of the samples at 4 K to UV radiation for PL experiments using the 275 nm line of an Ar ion laser at intensities of 10 W cm^{-2} did cause damage to the cap layer and on removal of the samples from the cryostat they were observed to have oxidized.

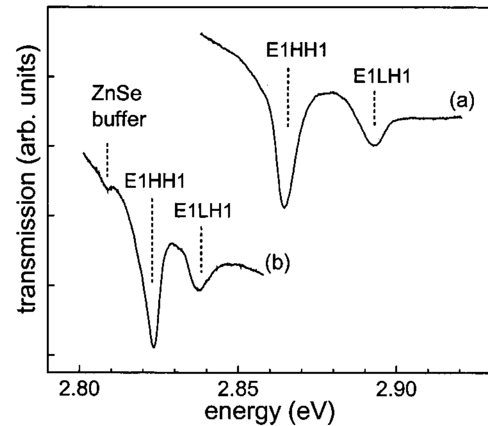

FIG. 4. Transmission spectra of multiple quantum-well structures with well widths: (a) 5.0 nm and (b) 10.0 nm. For (b) the contribution of the ZnSe buffer appears in the spectrum. The curves have been displaced vertically for clarity.

For optical transmission measurements samples containing ten quantum wells were grown with the structure ZnSe (buffer, 50 nm)/$10x$[MgS(5 nm) +ZnSe(L_w nm)]/MgS(20 nm)/ZnMgSSe cap and values of 5 and 10 nm were chosen for L_W where the contributions of the cap and buffer regions to the transmission signal are small compared to those of the quantum-well transitions. The transmission spectra were obtained using a halogen lamp as a white light source and a 0.75 m single spectrometer equipped with a 1200 lines/cm grating and recorded using a cooled charge-coupled device (CCD) camera after selectively removing the GaAs substrate by wet etching.

The high material quality of the two samples reported here is apparent from the transmission spectra at 4 K shown in Fig. 4. The heavy-hole exciton (E1HH1) and light-hole exciton ground-state transitions (E1LH1) are clearly visible for both the 5.0 [Fig. 4(a)] and 10.0 nm wide quantum wells [Fig. 4(b)]. The full width at half maximum (FWHM) values of the E1HH1 transitions for the 5.0 and 10.0 nm quantum-well samples are 11.0 and 6.2 meV, respectively, comparable to values typically obtained for the ZnSe/ZnCdSe and ZnMgSSe/ZnSe systems. The small inhomogeneous broadening indicates only minor well-width fluctuations and, in addition, the MgS/ZnSe system with two binary materials has the advantage of minimum alloy broadening.

A. Highly confined excitons

The stabilization of excitons at room temperature by the suppression of the exciton-LO phonon scattering is important for high-performance optoelectronic devices. For example, it is expected that an enhancement and a narrowing of the linewidth at room temperature of the excitonic absorption would be valuable in the case of modulators. Also, low-threshold

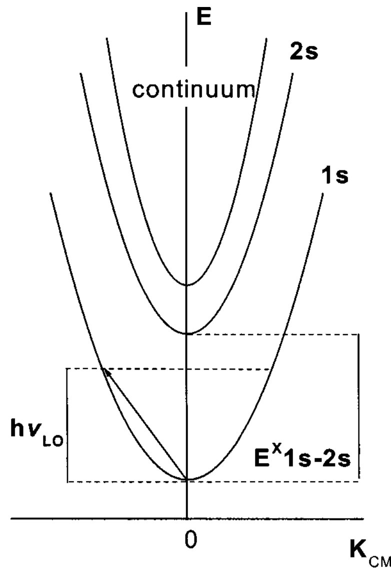

FIG. 5. Sketch of quantum-well exciton dispersion for a system with $E^X(1s-2s)>h\upsilon_{\rm LO}$.

laser emission should be possible with excitonic gain, which is much higher than that associated with a free electron-hole plasma. Laser emission due to excitonic and biexcitonic gain mechanisms has been observed in ZnSe-based structures by several groups[31,32,33] for temperatures up to 150 K. However, the strong interaction between the excitons and LO phonons usually results in the dissociation of the excitons at higher temperatures, reducing device efficiencies. Scattering of excitons by LO phonons leads to exciton dephasing resulting in broadening of the exciton-transition linewidth.

Ionization of excitons should be prevented in systems where all the excitations of the exciton have an energy larger than that of the LO phonon, namely, for $E^X(1s\text{-}2s)>h\upsilon_{\rm LO}$, due to the absence of final states for the scattering process[34] as shown in Fig. 5. However, although one might expect the relation $E^X(1s\text{-}2s)>h\upsilon_{\rm LO}$ to hold only in low-dimensional heterostructures such as those based on quantum wires and dots, it is clear that this phonon suppression can be achieved using MgS/ZnSe/MgS quantum wells, where large Rydberg values are expected due to a confinement potential of 2 eV.

B. Measurement of the exciton binding energies

The magneto-optics absorption experiments were carried out in an Oxford Instruments superconducting magnet capable of fields up to 14 T. A white light source was focussed onto the sample held in helium exchange gas at 4.2 K and the transmitted light was collected by an optical fiber and taken to the spectroscopy system described above.

In ZnSe the bulk exciton binding energy is 20 meV and the LO phonon energy is 32 meV.[35] Since the difference in bandgap between ZnSe (2.823 eV) and MgS (>4.8 eV) is in the order of 2 eV, the condition $E^X(1s\text{-}2s)>32\,\text{meV}$ is easily achievable in narrow quantum wells. Also, the large offset for both valence and conduction bands will prevent thermal escape of the carriers from the well to the barrier region.

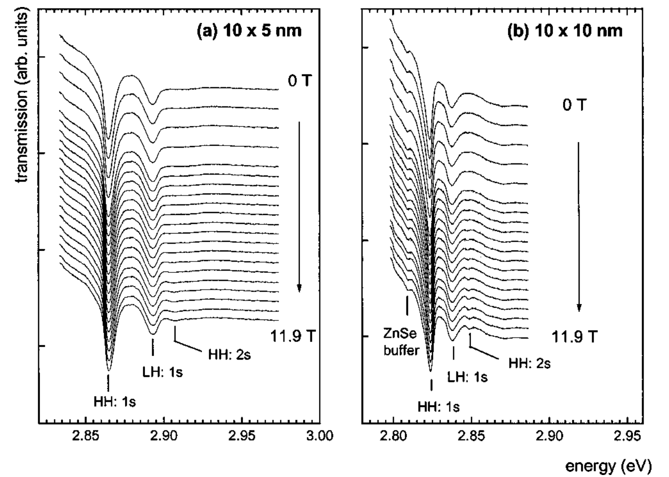

FIG. 6. Magnetotransmission of multiple ZnSe quantum wells with 5.0 nm (a) and 10.0 nm (b) thickness in MgS barriers

For a more detailed knowledge of the excitonic properties of this system the exciton binding energies were measured directly for the two samples shown in Fig. 4 by magnetotransmission, a technique already applied to the ZnSe/ZnCdSe by several authors.[36,37] The higher excited states of the excitons such as the $2s$ transitions are not visible in the zero-field transmission spectra but the oscillator strengths of the higher excited states of the excitons are increased when a magnetic field is applied parallel to the growth direction (Faraday geometry). The transitions are then detectable in the transmission spectra, as shown in Fig. 6, and these measured energies of the exciton absorption peaks are plotted against the magnetic-field strength in Fig. 7. We note that since unpolarized light was used the expected Zeeman splittings of the order of 0.5 meV (Ref. 38) were not observed. The exciton binding energy is obtained by extrapolating the transitions back to the zero-field values as shown in Fig. 7.

The magneto-exciton transitions are fitted using the model of Engbring and Zimmermann[39] that includes the effects of the confinement potential in the well, the Coulomb interaction and the magnetic field. The $1s$ exciton states remain nearly unaffected by the magnetic field as the carriers are

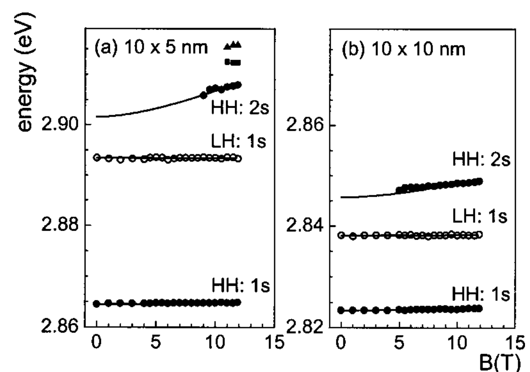

FIG. 7. Energy of exciton transitions versus magnetic field as measured by transmission for the same two samples shown in Fig. 6. The solid lines are a fit of the data with the model of Engbring and Zimmermann.[39]

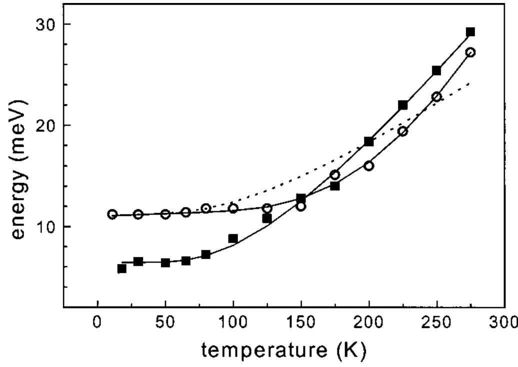

FIG. 8. FWHM of the heavy-hole exciton transitions versus temperature as measured by transmission and fitted with Eq. (4) for the same two samples shown in Fig. (4) with well widths: (○ and dotted line) 5.0 nm and (■ and solid line) 10.0 nm. The solid line through the measured values of the 5.0 nm well illustrates the two regimes discussed in the text.

tightly bound and the Coulomb interaction dominates over the magnetic-field effects. For the 5.0 and the 10.0 nm wide quantum-well samples the $2s$ heavy-hole exciton state emerges at higher fields and the values obtained for the zero field $1s$ to $2s$ heavy-hole exciton binding energy separations are 22.3 meV for the 10.0 nm well and 37.1 meV for the 5.0 nm well, hence the condition $E^X_{\mathrm{HH}}(1s-2s) > h\upsilon_{\mathrm{LO}}$ is fulfilled. Also, for the 5 nm well, the corresponding exciton binding energy of 43.9 meV corresponds to a remarkable enhancement by a factor of 2.2 compared with the bulk ZnSe value. This enhancement occurs because of the large difference in bandgaps and our calculations show that for the $1s$ exciton binding energy tunnelling effects only start to be significant at well widths below one monolayer. In the 10.0 nm wide quantum well the value for the $1s$ heavy-hole exciton binding energy of 28.3 meV is still larger than the bulk value, but the carriers are significantly less confined in this sample.

C. Exciton-LO phonon scattering

To verify directly the effect of the large exciton-binding energy on the stabilization of the exciton at higher temperature the line widths of the heavy-hole transitions were measured and the results are given in Fig. 8, where the FWHM of the heavy-hole exciton transitions is plotted versus temperature. The values were obtained from transmission spectra after removing the contributions of the buffer and cap layers. For individual exciton states the broadening can be written as

$$\Gamma = \Gamma_0 + \Gamma_{\mathrm{ac}} T + \Gamma_{\mathrm{LO}} [\exp(h\upsilon_{\mathrm{LO}/k_B T}) - 1]^{-1}, \tag{3}$$

where Γ_0 represents the inhomogeneous broadening, Γ_{ac} is the contribution due to the scattering with acoustic phonons and Γ_{LO} is the contribution due to the scattering with LO phonons. The values obtained by fitting the experimental data with Eq. (3) are summarized in Table II. For the fitting procedure, values of 3.0 μeV K^{-1} for the 10.0 nm sample and 5.0 μeV K^{-1} for the 5.0 nm sample were assumed for Γ_{ac}, in accordance with the work of Blewett *et al.*[38] and an LO-phonon energy of 32 meV was used. For the 10.0 nm wide quantum well the value for Γ_{LO} of 59.0 meV is very close to that of 60 meV reported for bulk ZnSe.[40] Fitting the temperature dependence for the 5 nm quantum well with Eq. (3) this value is reduced to 31.8 meV for the 5.0 nm wide well, which is in good agreement with a value of $\Gamma_{\mathrm{LO}}=34$ meV for a ZnSe (5.6 nm)/MgS(2.5 nm) superlattice obtained from temperature-dependent reflection spectroscopy.[10] As can be seen in Fig. 8 the fit obtained with Eq. (3) is poor for the 5 nm quantum well. Therefore, a second fit of the temperature dependence of the exciton linewidth with this equation was performed with the LO phonon energy as a fitting parameter to include phonon contributions from the MgS barrier. The best fit to the experimental data was obtained with a value of $\Gamma_{\mathrm{LO}}=342$ meV for a phonon energy of $h\upsilon_{\mathrm{LO}}=75$ meV, comparable to values for GaN with $\Gamma_{\mathrm{LO}}=375$ meV and $h\upsilon_{\mathrm{LO}}=91.7$ meV.[41] Although an interpretation involving scattering with phonons from the MgS barrier gives a better fit, this explanation is unlikely as very recently the MgS phonon energy has been measured by Raman spectroscopy to be 52 meV (Ref. 19), which does not agree with our fitted value of 75 meV. Also, the use of different phonon energies to fit the 5 and 10 nm quantum wells, which were grown identically apart from the different well thickness, is unphysical.

TABLE II. Parameters for the heavy-hole excitons obtained by fitting the magnetic field and temperature dependencies.

Well width (nm)	$E^X_{\mathrm{HH}}(1s-2s)$ (meV)	$E^X_{\mathrm{HH}}(1s)$ (meV)	Γ_0 (meV)	Γ_{LO} (meV)
5.0	37.1	43.9	11.0	31.8
10.0	22.3	28.3	6.2	59.0

The role of inhomogeneous broadening has to be taken explicitly into account as it seems possible to distinguish two different temperature regimes for the 5 nm sample. For temperatures up to 150 K the FWHM of the heavy-hole exciton remains unchanged, whereas for higher temperatures its dependence is similar to that of the 10 nm quantum well. These two regimes could correspond to a transition from the $E^X_{\mathrm{HH}}(1s-2s) > h\upsilon_{\mathrm{LO}}$ regime, where the exciton phonon scattering is suppressed, to the $E^X_{\mathrm{HH}}(1s\text{-}2s) < h\upsilon_{\mathrm{LO}}$ regime, where ionization occurs. The changeover is thought to be due to inhomogeneous broadening of the $1s$ exciton level and happens when delocalisation, possibly through scattering with acoustic phonons, becomes effective. Although $E^X_{\mathrm{HH}}(1s\text{-}2s) > h\upsilon_{\mathrm{LO}}$ holds for individual states the line widths of which are defined by their spatial extensions, this condition is not met by exciton levels broadened by around 10 meV after delocalization in the narrow quantum well sample. Therefore, the suppression of the exciton-LO phonon scattering is partial, and is only complete up to temperatures of approximately 150 K. It should be noted that the errors for determining the FWHM of the exciton transitions in absorption spectra increase with temperature. Further studies on a larger number of samples are needed to allow a better description of the influence of quantum confinement on the exciton-LO phonon scattering process.

VI. CONCLUSIONS

A MBE growth technique has been used to grow thick layers of zincblende MgS. The method involves the use of ZnS and Mg sources so that at the surface the Mg replaces the Zn and only a small residual Zn remains in the MgS layer. The kinetics of the reaction are discussed and it is concluded that the residual concentrations of Zn are not an equilibrium concentration but is determined by the kinetics of the reaction.

High quality single and multiple quantum-well structures have been grown and characterized by optical spectroscopy. The absorption line widths are comparable with ZnSe/ZnCdSe quantum wells and magneto-optical measurements have provided a direct measurement of the exciton binding energies for samples with different ZnSe well widths in MgS barriers. For a 5 nm well a value of 43.9 meV was obtained and is the largest value reported for this material system. In this sample, the exciton binding energy, $E^X(1s\text{-}2s) > h\upsilon_{\mathrm{LO}}$ and due to the absence of final states of scattering, the broadening of the transitions due to LO-phonon scattering in this sample should be diminished due to the suppression of the exciton-LO phonon scattering. In fact, the value of the FWHM of the HH exciton transition linewidth for the 5.0 nm quantum well is constant up to 150 K indicating a strong decrease of the exciton-LO phonon scattering process in this regime.

---

*Present address: Marconi Communications, Cambridge Business Park, Milton Road, Cambridge CB4 0WZ, UK.

†Present address: Center de Recherche sur l'Hetero-Epitaxie et ses Applications, Center National de la Recherche Scientifique (CRHEA/CNRS), Rue Bernard Gregory, F-06560 Valbonne-Sophia-Antipolis, France.

[1] A. Navrotsky and J. C. Phillips, Phys. Rev. B **11**, 1583 (1975).

[2] A. Lichanot, A. Dargelos, C. Larrieu, and R. Orlando, Solid State Commun. **90**, 189 (1994).

[3] S. Ekbundit, A. Chizmeshya, R. La Violette, and G. H. Wolf, J. Phys.: Condens. Matter **8**, 8251 (1996).

[4] G. Kalpana, B. Palanivel, R. T. Thomas, and M. Rajagopalan, Physica B **222**, 223 (1996).

[5] H. Kimijima, M. Kitagawa, R. Inoue, N. Shiraishi, M. Hoashi, K. Ichino, H. Kobayashi, Appl. Surf. Sci. **113/114**, 432 (1997).

[6] N. Teraguchi, H. Mouri, Y. Tomomura, A. Suzuki, H. Taniguchi, J. Rorison, and G. Duggan, Appl. Phys. Lett. **67**, 2945 (1995).

[7] L. Konczewicz, P. Bigenwald, T. Cloitre, M. Chibane, R. Ricou, P. Testud, O. Briot, and R. L. Aulombard, J. Cryst. Growth **159**, 117 (1996).

[8] K. Uesugi, T. Obinata, H. Kumano, J. Nakahara, and I. Suemune, Appl. Phys. Lett. **68**, 844 (1996).

[9] H. Nashiki, I. Suemune, H. Kumano, H. Suzuki, T. Obinata, K. Uesugi, and J. Nakahara, Appl. Phys. Lett. **70**, 2350 (1997).

[10] H. Kumano, H. Nashiki, I. Suemune, M. Arita, T. Obinata, H. Suzuki, K. Uesugi, and J. Nakahara, Phys. Rev. B **55**, 4449 (1997).

[11] C. Bradford, C. B. O'Donnell, B. Urbaszek, A. Balocchi, C. Morhain, K. A. Prior, and B. C. Cavenett, Appl. Phys. Lett. **76**, 3929 (2000).

[12] L. H. Kuo, L. Salamanca-Riba, B. J. Wu, G. E. Höfler, J. M. DePuydt, and H. Cheng, Appl. Phys. Lett. **67**, 3298 (1995).

[13] L. H. Kuo, K. Kimura, T. Yasuda, S. Miwa, C. G. Jin, K. Tanaka, and T. Yao, Appl. Phys. Lett. **68**, 2413 (1996).

[14] L. Tapfer and K. Ploog, Phys. Rev. B **40**, 9802 (1989).

[15] H. Holloway, J. Appl. Phys. **67**, 6229 (1990).

[16] B. K. Tanner, J. Phys. D **26**, A151 (1993).

[17] C. B. O'Donnell, C. Bradford, K. A. Prior, and B. C. Cavenett (unpublished).

[18] T.-Y. Chung, J. H. Oh, S.-G. Lee, J.-W. Jeong, and K. J. Chang, Semicond. Sci. Technol. **12**, 701 (1997).

[19] D. Wolverson, D. M. Bird, C. Bradford, K. A. Prior, and B. C. Cavenett, Phys. Rev. B **64**, 113203 (2001).

[20] S. Froyen, S.-H. Wei, and A. Zunger, Phys. Rev. B **38**, 10124 (1988).

[21] H. Okuyama, K. Nakano, T. Miyajima, and K. Akimoto, Jpn. J. Appl. Phys. **30**, L1620 (1991).

[22] P. Boguslawski, Solid State Commun. **57**, 623 (1986).

[23] S.-G. Lee and K. J. Chang, Phys. Rev. B **52**, 1918 (1995).

[24] W. A. Jesser, Mater. Sci. Eng. **4**, 279 (1969).

[25] R. Bruinsma and A. Zangwill, J. Physique **47**, 2055 (1986).

[26] S. Guha, B. J. Wu, H. Cheng, and J. M. DePuydt, Appl. Phys. Lett. **63**, 2129 (1993).

[27] S. V. Ivanov, S. V. Sorokin, P. S. Kop'ev, J. R. Kim, H. D. Jong, and H. S. Park, J. Cryst. Growth **159**, 16 (1996).

[28] O. Kubaschewski, C. B. Alcock, and P. J. Spencer, *Materials Thermochemistry*, 6th ed. revised (Pergamon, Oxford, 1993).

[29] K. A. Prior, G. J. Davies, and R. Heckingbottom, J. Cryst. Growth **66**, 55 (1984).

[30] V. S. Sorokin, S. V. Sorokin, V. A. Kaygorodov, and S. V. Ivanov, J. Cryst. Growth **214-215**, 130 (2001).

[31] M. Dabbicco, M. Lepore, R. Cingolani, G. Scamarcio, M. Ferrara, and I. Suemune, Semicond. Sci. Technol. **7**, 681 (1992).

[32] Y. Kawakami, I. Hauksson, H. Stewart, J. Simpson, I. Galbraith, K. A. Prior, and B. C. Cavenett, Phys. Rev. B **48**, 11 994 (1993).

[33] Y. Kuroda, I. Suemune, Y. Fujii, and M. Fujimoto, Appl. Phys. Lett. **61**, 1182 (1992).

[34] S. Nojima, Phys. Rev. B **46**, 2302 (1992).

[35] H. E. Gumlich, D. Theis, and D. Tschierse, in *Physics of II-VI and I-VII Compounds, Semimagnetic Semiconductors*, edited by O. Madelung, Landolt-Börnstein, New Series, Group III, Vol. 17b (Springer Verlag, Berlin, 1982), Chap. 3.7.

[36] J. Puls, V. V. Rossin, F. Henneberger, and R. Zimmermann, Phys. Rev. B **54**, 4974 (1996).

[37] A. De Nardis, V. Pelligrini, R. Colombelli, F. Beltram, L. Vanzetti, A. Franciosi, I. N. Krivorotov, and K. K. Bajaj, Phys. Rev. B **61**, 1700 (2000).

[38] I. J. Blewett, D. I. Bain, A. Tookey, G. Brown, I. Galbraith, A. K. Kar, B. Vögele, K. A. Prior, B. C. Cavenett, and B. S. Wherrett, Phys. Rev. B **59**, 9756 (1999).

[39] J. Engbring and R. Zimmermann, Phys. Status Solidi B **173**, 733 (1992).

[40] N. T. Pelekanos, J. Ding, M. Hagerott, A. V. Nurmiko, H. Luo, N. Samarth, and J. K. Furdyna, Phys. Rev. B **45**, 6037 (1992).

[41] A. J. Fischer, W. Shan, J. J. Song, Y. C. Chang, R. Horning, and B. Goldenberg, Appl. Phys. Lett. **71**, 1981 (1997).